ISME2010-2866

A finite strain SMA constitutive model: comparison of small and finite strain formulations

J. Arghavani[1], F. Auricchio[2,3,4], R. Naghdabadi[1,5], A. Reali[2,3]

[1] Department of Mechanical Engineering, Sharif University of Technology, Tehran, Iran
[2] Dipartimento di Meccanica Strutturale, Università degli studi di Pavia, Pavia, Italy
[3] Istituto di Matematica Applicata e Tecnologie Informatiche del CNR, Pavia, Italy
[4] European Centre for Training and Research in Earthquake Engineering (EUCENTRE), Pavia, Italy
[5]Institute for Nano-Science and Technology, Sharif University of Technology, Tehran, Iran

Abstract
In this paper, we investigate the finite strain formulation of a previously proposed model for shape memory alloys in the small strain regime. The derivation is based on the multiplicative decomposition of the deformation gradient into elastic and transformation parts and utilizing the thermodynamics of irreversible process with internal variables. Some boundary value problems are considered to compare the effects of finite deformation in shape memory alloys-based structures. Finally we discuss on the limitation of small-strain based constitutive models in simulating shape memory alloy devices.

Keywords: Shape memory alloys, finite strain, constitutive model, internal variables

Introduction

Smart materials are well-known materials exhibiting special properties, known as pseudo-elasticity (or super-elasticity), one-way and two-way shape memory effects [1,2], suitable for industrial applications and engineering. For example, nowadays pseudo-elastic Nitinol is a common and well-known engineering material in the medical industry [3].

The origin of SMA features is a reversible thermo-elastic martensitic phase transformation between a high symmetry, austenitic phase and a low symmetry, martensitic phase. Austenite is a solid phase, usually characterized by a body-centered cubic crystallographic structure, which transforms into martensite by means of a lattice shearing mechanism. When the transformation is driven by a temperature decrease, martensite variants compensate each other, resulting in no macroscopic deformation. However, when the transformation is driven by the application of a load, specific martensite variants, favorable to the applied stress, are preferentially formed, exhibiting a macroscopic shape change in the direction of the applied stress. Upon unloading or heating, this shape change disappears through the reversible conversion of the martensite variants into the parent phase [1,4].

The starting and finishing temperatures of a stress-free SMA during forward transformation (austenite to martensite), A_s and A_f, as well as the starting and finishing temperatures during reverse transformation, M_s and M_f, are the four characteristic temperatures for a shape memory alloy. In a stress-free condition, at a temperature above A_f, only austenitic phase is stable, while martensite is stable only at a temperature below M_f. Applying a stress at a temperature above A_f, SMAs exhibit pseudo-elastic behavior with a full recovery of inelastic strain upon unloading. Instead, at a temperature below M_f, the material presents the shape memory effect with permanent inelastic strains upon unloading which may be recovered by heating.

In most applications, SMAs experience general thermo-mechanical loads, which are more complicated than uniaxial or multiaxial proportional loadings, and typically undergo large rotations and moderate strains (i.e., in the range of 10% for polycrystals [1]). For example, with reference to biomedical applications, stent structures are usually designed to significantly reduce their diameter during the insertion into a catheter; thereby, large rotations combined with moderate strains occur and the use of a finite deformation scheme is preferred.

The majority of the current 3D macroscopic constitutive models of SMA have been developed in the pseudo-elastic range and small deformation regime [5-12]. Finite deformation SMA constitutive models available in the literature have been mainly developed by extending small strain constitutive models. The approach in most of the cases is based on the multiplicative decomposition of the deformation gradient into an elastic and an inelastic or transformation part [12-15], although there are some models in the literature which have utilized an additive decomposition of the strain rate tensor into an elastic and an inelastic part [16].

Recently, Evangelista et al. [15] have extended the small strain constitutive model proposed by Souza et al. [11] and discussed by Auricchio and Petrini [6] to the finite deformation regime. The small strain constitutive model has been deeply discussed by Auricchio and Petrini [6,7]. In this paper, considering different boundary value problems, we compare the small-strain and the finite-strain constitutive models.

The paper is organized as follows. In Section 2, based on a multiplicative decomposition of the deformation gradient into elastic and transformation parts, we present the finite strain constitutive model. Section 3 presents the time-discrete frame for of the evolution equation as well as the solution algorithm. In Section 4 we solve different boundary value problems and

compare the small and finite strain formulations. Finally in Section 5 we draw conclusions.

A 3D finite strain SMA constitutive model

Following references [12,15], and taking into consideration the small-strain constitutive model in [6], we adopt a 3D finite-strain constitutive model within the framework of continuum thermodynamics with internal variables.

Considered a deformable body, we denote with $\mathbf{F}$ the deformation gradient and with J its determinant, supposed to be positive. The tensor $\mathbf{F}$ can be uniquely decomposed as:

$$\mathbf{F} = \mathbf{RU} = \mathbf{VR} \tag{1}$$

where $\mathbf{U}$ and $\mathbf{V}$ are the right and left stretch tensors, respectively, both positive definite and symmetric, while $\mathbf{R}$ is a proper orthogonal rotation tensor. The right and left Cauchy-Green deformation tensors are then respectively defined as:

$$\mathbf{C} = \mathbf{F}^T\mathbf{F},\ \mathbf{b} = \mathbf{F}\mathbf{F}^T \tag{2}$$

and the Green-Lagrange strain tensor, $\mathbf{E}$, reads as:

$$\mathbf{E} = \frac{\mathbf{C}-\mathbf{1}}{2} \tag{3}$$

where $\mathbf{1}$ is the second-order identity tensor. Moreover, the velocity gradient tensor $\mathbf{L}$ is given as:

$$\mathbf{L} = \dot{\mathbf{F}}\mathbf{F}^{-1} \tag{4}$$

The symmetric and anti-symmetric parts of $\mathbf{L}$ supply the strain rate tensor $\mathbf{d}$ and the vorticity $\mathbf{w}$, i.e.:

$$\mathbf{d} = \frac{1}{2}(\mathbf{L}+\mathbf{L}^T),\ \mathbf{w} = \frac{1}{2}(\mathbf{L}-\mathbf{L}^T) \tag{5}$$

Taking the time derivative of equation (3) and using (4) and (5), it can be shown that:

$$\dot{\mathbf{E}} = \mathbf{F}^T\mathbf{d}\mathbf{F} \tag{6}$$

The second Piola-Kirchhoff stress tensor $\mathbf{S}$ is obtained from the Cauchy stress as:

$$\mathbf{S} = J\mathbf{F}^{-1}\sigma\mathbf{F}^{-T} \tag{7}$$

Following a well-stablished approach adopted in plasticity, we assume a local multiplicative decomposition of the deformation gradient into an elastic part $\mathbf{F}^e$, defined with respect to an intermediate configuration, and a transformation one $\mathbf{F}^t$, defined with respect to the reference configuration. Accordingly:

$$\mathbf{F} = \mathbf{F}^e\mathbf{F}^t \tag{8}$$

Since experimental evidences indicate that the transformation flow is nearly isochoric, we have to impose $\det(\mathbf{F}^t) = 1$, which after taking the time derivative results in $tr(\mathbf{d}^t) = 0$.

We define $\mathbf{C}^e = \mathbf{F}^{eT}\mathbf{F}^e$ and $\mathbf{C}^t = \mathbf{F}^{tT}\mathbf{F}^t$ as the elastic and the transformation right Cauchy-Green tensors and, using definition (2) and (8), we obtain:

$$\mathbf{C}^e = \mathbf{F}^{t-T}\mathbf{C}\mathbf{F}^{t-1} \tag{9}$$

In order to satisfy the principle of material objectivity, the Helmholtz free energy has to depend on $\mathbf{F}^e$ only through the elastic right Cauchy-Green strain tensor; it is moreover assumed to be a function of the transformation strain, $\mathbf{E}^t = (\mathbf{C}^t - \mathbf{1})/2$, and of the temperature in the following form:

$$\Psi = \Psi\left(\mathbf{C}^e, \mathbf{E}^t, T\right) = W(\mathbf{C}^e) + \psi(\mathbf{E}^t, T) \tag{10}$$

where, $W(\mathbf{C}^e)$ is a hyperelastic strain energy function. In addition, we assume $W(\mathbf{C}^e)$ to be an isotropic function of $\mathbf{C}^e$ and to be the same for austenite and martensite phases; it can be therefore expressed as $W(\mathbf{C}^e) = W(I_{\mathbf{C}^e}, II_{\mathbf{C}^e}, III_{\mathbf{C}^e})$, where $I_{\mathbf{C}^e}, II_{\mathbf{C}^e}, III_{\mathbf{C}^e}$ are the invariants of $\mathbf{C}^e$. We also define ψ in the following form [6-8,11]

$$\psi(\mathbf{E}^t, T) = \tau_M \| \mathbf{E}^t \| + \frac{1}{2}h \| \mathbf{E}^t \|^2 + \mathcal{I}_{\varepsilon_L}(\| \mathbf{E}^t \|) \tag{11}$$

where $\tau_M = \beta < T - T_0 >$ and β, T_0 and h are material parameters, while the MacCauley brackets calculate the positive part of the argument, i.e. $< x >= (x + |x|)/2$, and the norm operator is defined as $\| \mathbf{A} \| = \sqrt{\mathbf{A} : \mathbf{A}^T}$, with $\mathbf{A} : \mathbf{B} = A_{ij}B_{ij}$.

Moreover, in equation (11) we also use the indicator function $\mathcal{I}_{\varepsilon_L}$ defined as:

$$\mathcal{I}_{\varepsilon_L}(\| \mathbf{E}^t \|) = \begin{cases} 0 & \text{if } \| \mathbf{E}^t \| \le \varepsilon_L \\ +\infty & \text{otherwise} \end{cases} \tag{12}$$

in order to satisfy the constraint on the transformation strain norm (i.e., $\| \mathbf{E}^t \| \le \varepsilon_L$). The material parameter ε_L is the maximum transformation strain norm in a uniaxial test.

Taking the time derivative of equation (9) and using (4), the material time derivative of the elastic right Cauchy-Green deformation tensor is obtained as:

$$\dot{\mathbf{C}}^e = -\mathbf{L}^{tT}\mathbf{C}^e + \mathbf{F}^{t-T}\dot{\mathbf{C}}\mathbf{F}^{t-1} - \mathbf{C}^e\mathbf{L}^t \tag{13}$$

We now use Clausius-Duhem inequality form of the second law of thermodynamics:

$$\mathbf{S} : \dot{\mathbf{E}} - (\dot{\Psi} + \eta\dot{T}) \ge 0 \tag{14}$$

Substituting (10) into (14) we obtain:

$$\mathbf{S} : \frac{1}{2}\dot{\mathbf{C}} - \frac{\partial W}{\partial \mathbf{C}^e} : \dot{\mathbf{C}}^e - \frac{\partial \psi}{\partial \mathbf{E}^t} : \dot{\mathbf{E}}^t - \frac{\partial \psi}{\partial T}\dot{T} \ge 0 \tag{15}$$

Substituting (13) into (15), after some mathematical manipulations, we obtain:

$$\begin{aligned} &\left(\mathbf{S} - 2\mathbf{F}^{t-1}\frac{\partial W}{\partial \mathbf{C}^e}\mathbf{F}^{t-T}\right) : \frac{1}{2}\dot{\mathbf{C}} - \left(\eta + \frac{\partial \psi}{\partial T}\right)\dot{T} \\ &\quad + 2\mathbf{C}^e\frac{\partial W}{\partial \mathbf{C}^e} : \mathbf{L}^t - \mathbf{X} : \dot{\mathbf{E}}^t \ge 0 \end{aligned} \tag{16}$$

where

$$\mathbf{X} = \frac{\partial \psi}{\partial \mathbf{E}^t} = \left(\tau_M + h \| \mathbf{E}^t \| + \gamma\right)\frac{\mathbf{E}^t}{\| \mathbf{E}^t \|} \tag{17}$$

The positive variable γ results from the indicator function subdifferential $\partial \mathcal{I}_{\varepsilon_L}(\mathbf{E}^t)$ and it is defined as:

$$\gamma = \begin{cases} \gamma & if \quad \| \mathbf{E}^t \| = \varepsilon_L \\ 0 & otherwise \end{cases} \tag{18}$$

We also use the isotropic property of $W(\mathbf{C}^e)$, implying that $\mathbf{C}^e$ and $\dfrac{\partial W}{\partial \mathbf{C}^e}$ are coaxial. Following standard arguments, we may finally conclude:

$$\mathbf{S} = 2\mathbf{F}^{t-1} \frac{\partial W}{\partial \mathbf{C}^e} \mathbf{F}^{t-T}, \ \eta = -\frac{\partial \psi}{\partial T} \tag{19}$$

Utilizing equation (16), and using the classical property of second-order tensor double contraction $\mathbf{A} : (\mathbf{BC}) = \mathbf{B} : (\mathbf{AC}^T) = \mathbf{C} : (\mathbf{B}^T \mathbf{A})$, we conclude:

$$\mathbf{X} : \dot{\mathbf{E}}^t = \left(\mathbf{F}^t \mathbf{X} \mathbf{F}^{tT} \right) : \mathbf{d}^t \tag{20}$$

Substituting (19) and (20) into (16), the dissipation inequality can be written as:

$$(\mathbf{P} - \mathbf{K}) : \mathbf{d}^t \geq 0 \tag{21}$$

where

$$\mathbf{P} = 2\mathbf{C}^e \frac{\partial W}{\partial \mathbf{C}^e}, \quad \mathbf{K} = \mathbf{F}^t \mathbf{X} \mathbf{F}^{tT} \tag{22}$$

In order to satisfy the second law of thermodynamics, (21), we may define the following evolution equation:

$$\mathbf{d}^t = \dot{\zeta} \frac{(\mathbf{P} - \mathbf{K})^D}{\| (\mathbf{P} - \mathbf{K})^D \|} \tag{23}$$

which also satisfies the inelastic deformation incompressibility condition. We highlight that we indicate with a superscript D the deviatoric part of a tensor. In order to describe phase transformation, we choose the following limit function:

$$f = \| (\mathbf{P} - \mathbf{K})^D \| - R \tag{24}$$

where the elastic region radius, R, is a material parameter.

Similarly to plasticity, the consistency parameter and the limit function satisfy the Kuhn-Tucker conditions:

$$f \leq 0, \ \dot{\zeta} \geq 0, \ \dot{\zeta} f = 0 \tag{25}$$

Representation with respect to the reference configuration

In the previous section, using a multiplicative decomposition of the deformation gradient into elastic and transformation parts, we derived a finite-strain constitutive model. But while $\mathbf{F}$ and $\mathbf{F}^t$ are related to the reference configuration, $\mathbf{F}^e$ has been defined with respect to an intermediate configuration. It is however necessary to recast all equations in terms of quantities described with respect to the reference configuration, so that all equations are Lagrangian.

Since a hyperelastic strain energy function $W(\mathbf{C}^e)$ has been introduced in terms of $\mathbf{C}^e$ (i.e. with respect to the intermediate configuration), we first investigate it.

As introduced before, W depends on $\mathbf{C}^e$ only through its invariants. But the invariants of $\mathbf{C}^e$ are equal to those of $\mathbf{CC}^{t-1}$, as we show for the first invariant (the same can be shown also for the second and the third invariants in a similar way):

$$\begin{aligned} I_{\mathbf{C}^e} &= tr(\mathbf{C}^e) = tr\left(\mathbf{F}^{t-T} \mathbf{C} \mathbf{F}^{t-1} \right) \\ &= tr\left(\mathbf{C} \mathbf{F}^{t-1} \mathbf{F}^{t-T} \right) = tr\left(\mathbf{C} \mathbf{C}^{t-1} \right) = I_{\mathbf{CC}^{t-1}} \end{aligned} \tag{26}$$

According to the representation theorem, we may now write:

$$\frac{\partial W}{\partial \mathbf{C}^e} = \alpha_1 \mathbf{I} + \alpha_2 \mathbf{C}^e + \alpha_3 \mathbf{C}^{e2} \tag{27}$$

where $\alpha_i = \alpha_i (I_{\mathbf{CC}^{tr-1}}, II_{\mathbf{CC}^{t-1}}, III_{\mathbf{CC}^{t-1}})$.

Substituting (27) into $(19)_1$, we conclude that:

$$\mathbf{S} = 2\left(\alpha_1 \mathbf{C}^{t-1} + \alpha_2 \mathbf{C}^{t-1} \mathbf{C} \mathbf{C}^{t-1} + \alpha_3 \mathbf{C}^{t-1} \left(\mathbf{C} \mathbf{C}^{t-1} \right)^2 \right) \tag{28}$$

which expresses the second Piola-Kirchhoff stress tensor in terms of the quantities computed with respect to the reference configuration.

In order to find the Lagrangian form of the evolution equation, we substitue (23) into (6) and obtain:

$$\dot{\mathbf{E}}^t = \dot{\zeta} \mathbf{F}^{tT} \frac{(\mathbf{P} - \mathbf{K})^D}{\| (\mathbf{P} - \mathbf{K})^D \|} \mathbf{F}^t \tag{29}$$

or equivalently,

$$\dot{\mathbf{C}}^t = 2\dot{\zeta} \mathbf{F}^{tT} \frac{(\mathbf{P} - \mathbf{K})^D}{\| (\mathbf{P} - \mathbf{K})^D \|} \mathbf{F}^t \tag{30}$$

We now consider the first term in (30) and we compute:

$$\begin{aligned} \mathbf{F}^{tT} \mathbf{P} \mathbf{F}^t &= \left(\mathbf{F}^t \mathbf{C}^e \mathbf{F}^t \right) \left(2\mathbf{F}^{t-1} \frac{\partial W}{\partial \mathbf{C}^e} \mathbf{F}^{t-T} \right) \mathbf{C}^t \\ &= \mathbf{CSC}^t \end{aligned} \tag{31}$$

Considering the second term, we obtain:

$$\mathbf{F}^{tT} \mathbf{K} \mathbf{F}^t = \mathbf{F}^{tT} \mathbf{F}^t \mathbf{X} \mathbf{F}^{tT} \mathbf{F}^t = \mathbf{C}^t \mathbf{X} \mathbf{C}^t \tag{32}$$

We now define:

$$\mathbf{Y} \mathbf{C}^t = \mathbf{F}^{tT} (\mathbf{P} - \mathbf{K}) \mathbf{F}^t \tag{33}$$

and obtain from (31)-(33):

$$\mathbf{Y} = \mathbf{CS} - \mathbf{C}^t \mathbf{X} \tag{34}$$

Moreover, it can be easily shown that:

$$\| (\mathbf{P} - \mathbf{K})^D \| = \| \mathbf{Y}^D \| \tag{35}$$

Now, we substitute (33) and (35) into (30) and (24) to obtain:

$$f = \| \mathbf{Y}^D \| - R \tag{36}$$

and

$$\dot{\mathbf{C}}^t = 2\dot{\zeta} \frac{\mathbf{Y}^D}{\| \mathbf{Y}^D \|} \mathbf{C}^t = \dot{\zeta} \mathbf{A} \tag{37}$$

where $\mathbf{A} = 2 \dfrac{\mathbf{Y}^D}{\| \mathbf{Y}^D \|} \mathbf{C}^t$.

In this study, we use the commonly used Saint-Venant Kirchhoff strain energy function:

$$W = \frac{\lambda}{2} \left(tr \mathbf{E}^e \right)^2 + G \, tr \mathbf{E}^{e2} \tag{38}$$

which yields:

$$\alpha_1 = \frac{\lambda}{4}\left(\mathbf{C}:\mathbf{C}^{t-1}-3\right)-\frac{1}{2}G, \alpha_2 = \frac{1}{2}G, \alpha_3 = 0 \quad (39)$$

where λ and G are Lame constants.

Solution algorithm

In this section, the constitutive model as it has been derived in Section 2 will be prepared for the use in a finite element program. We now treat the non-linear problem described in Section 2 as an implicit time-discrete deformation-driven problem. Accordingly, we subdivide the time interval of interest $[0,T]$ in sub-increments and we solve the evolution problem over the generic interval $[t_n, t]$ with $t > t_n$.

The exponential map integration scheme has been up to now applied to problems of plasticity and isotropic inelasticity. The use of the exponential map enables to exactly conserve the inelastic volume. Thus, it allows larger time step sizes than any other first-order accurate integration scheme. Following [12], we obtain the following time-discrete form of the evolution equation:

$$\mathbf{C}_n^{t-1} = \mathbf{U}^{t-1}\exp\left(\Delta\zeta\mathbf{U}^{t-1}\mathbf{A}\mathbf{U}^{t-1}\right)\mathbf{U}^{t-1} \quad (40)$$

As it is usual in computational inelasticity problems, we also use an elastic-predictor inelastic-corrector procedure to solve the time-discrete constitutive model. The algorithm consists of evaluating an elastic trial state, in which the internal variable remains constant, and in verifying the admissibility of the trial function. If the trial state is admissible, the step is elastic; if the trial state is non-admissible the step is inelastic and the transformation internal variable should be updated through integration of the evolution equation.

In order to solve the inelastic step, we use another predictor-corrector scheme, that is we assume $\gamma = 0$ (which means we predict transformation strain is not saturated and $\| \mathbf{E}^t \| \leq \varepsilon_L$) and solve the following system of equations:

$$\begin{cases} \mathbf{R}^t = -\mathbf{C}_n^{t-1} + \mathbf{U}^{t-1}\exp\left(\Delta\zeta\mathbf{U}^{t-1}\mathbf{A}\mathbf{U}^{t-1}\right)\mathbf{U}^{t-1} = \mathbf{0} \\ R^\zeta = \| \mathbf{Y}^D \| - R = 0 \end{cases} \quad (41)$$

Then we solve the seven nonlinear scalar equations with a Newton-Raphson method.

If the solution is not admissible (i.e., $\| \mathbf{E}^t \| > \varepsilon_L$), we assume $\gamma > 0$ and the following saturated system is solved:

$$\begin{cases} \mathbf{R}^t = -\mathbf{C}_n^{t-1} + \mathbf{U}^{t-1}\exp\left(\Delta\zeta\mathbf{U}^{t-1}\mathbf{A}\mathbf{U}^{t-1}\right)\mathbf{U}^{t-1} = \mathbf{0} \\ R^\zeta = \| \mathbf{Y}^D \| - R = 0 \\ R^\gamma = \| \mathbf{E}^t \| - \varepsilon_L = 0 \end{cases} \quad (42)$$

We note that the variable $\mathbf{X}$ is not defined for the case of vanishing transformation strain. We use a regularization scheme for the norm to overcome this problem [10]:

$$\overline{\| \mathbf{E}^t \|} = \sqrt{\| \mathbf{E}^t \|^2 + \delta} \quad (43)$$

where δ is a user defined regularization parameter.

Boundary value problems

In order to simulate different boundary value problems, we have implemented the finite-strain constitutive model in a user-defined subroutine (UMAT) in the nonlinear finite element software ABAQUS. Moreover, we have implemented the small-strain constitutive model which is obtained by linearizing the finite-strain constitutive model [17]. For more details on finite-strain constitutive model numerical implementation, see [18].

We simulate some boundary value problems and compare the small strain and the finite strain constitutive models. We first simulate tension test, which is a simple case without any rotation effects, and can demonstrate the model differences due to strain regime (and not due to large rotations). In the second simulation, we study a cantilever beam problem and compare the results for different formulations. Finally we simulate an arc-shaped beam under an out-of-plane force which induces both torsion and bending in the structure.

In all comparisons, we use three formulations: small strain, small rotation formulation; small strain, finite rotation formulation; and finite deformation formulation (finite strain and finite rotation). We name the formulations SSSR, SSFR and FSFR, respectively. In SSFR formulation, we use a corotational formulation.

In all simulations, we use the material properties presented in Table 1.

Table 1 - Material parameters for a SMA

Parameter	Value	Unit
E	50000	MPa
ν	0.33	---
h	3000	MPa
ε_L	0.05	---
τ_M	200	MPa/K
R	100	MPa

Example 1: We simulate a simple tension test for a rod with L = 100 mm, h = 6 mm and b = 8 mm (Figure 1) and with an applied displacement at one end (up to 7 mm which is unloaded to the initial configuration), while another end is fixed (we will then use the geometry for the beam in the second example). Figure 2 presents the simulation results as well as different formulation comparisons. According to Figure 2, we conclude that all formulations result in approximately the same behavior. For displacements larger than 4 mm, there is a small difference between small-strain and finite-strain formulation results.

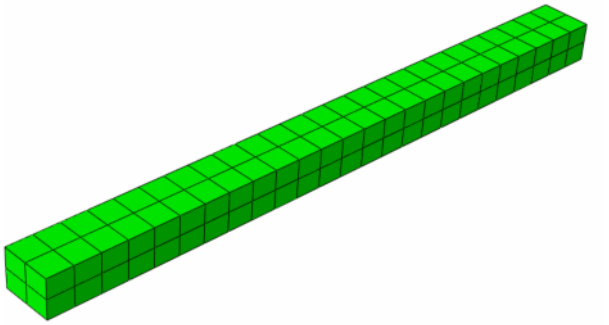

Figure 1. geometry and mesh in examples 1 and 2

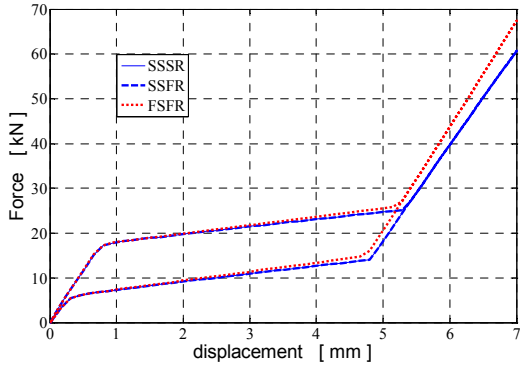

Figure 2. force-displacement diagram and comparison of different formulations under tension test.

Example 2: We now simulate a cantilever beam which is loaded at the end by a force F = 2000 N and then unloaded. Figure 3 shows the deformed shape when a finite-strain formulation is used. Figure 4 shows the force-displacement (component in the direction of the force) curve as well as different formulation comparisons, highlighting the big difference between the SSSR response and the finite rotation one.

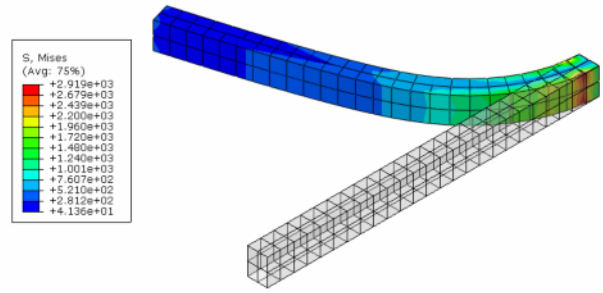

Figure 3. the cantilever beam under tip force, deformed shape when FSFR formulation is used.

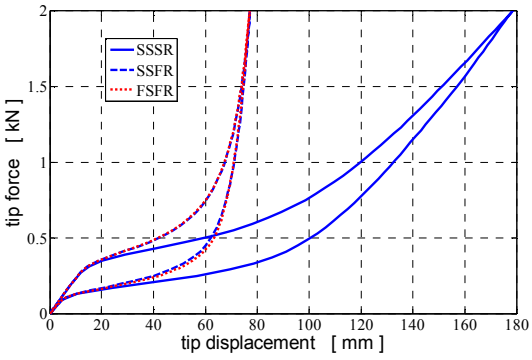

Figure 4. force-tip displacement diagram for the cantilever beam and different formulations comparison.

Example 3: We finally simulate the arc-shaped beam shown in Figure 5 with an outer radius of 20 mm, an inner radius of 15 mm and a thickness of 2mm subjected to an out-of- plane force of 500 N.

Figure 6 shows the deformed shape under the maximum force of 500 N. In Figure 7, we show the force-displacement diagrams. We remark that, in Figure 7, displacement vector magnitude has been reported.

According to the simulation results we conclude that, using a small-strain formulation without considering rotation effects, may lead to highly unsatisfactory results. Moreover we can observe that, using a small-strain formulation and considering the rotation effects in a corotational formulation can improve the results in the same way as a full finite-strain formulation can do. While both SSFR and FSFR formulations yields approximately the same results, the computational cost in terms of CPU time is much lower for the corotational formulation. This is an important issue from a computational cost point of view.

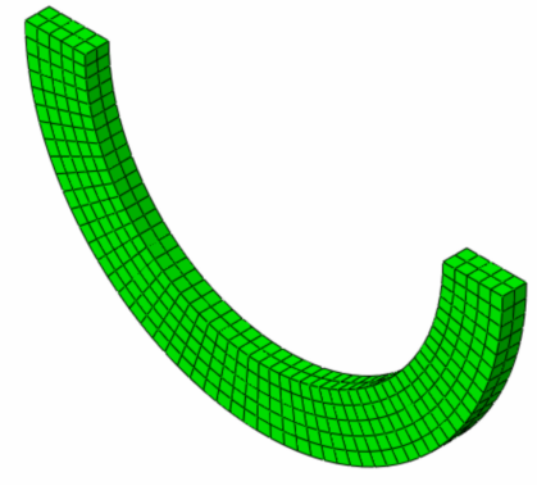

Figure 5. geometry and mesh description in the arc-shaped beam example under an out of plane force.

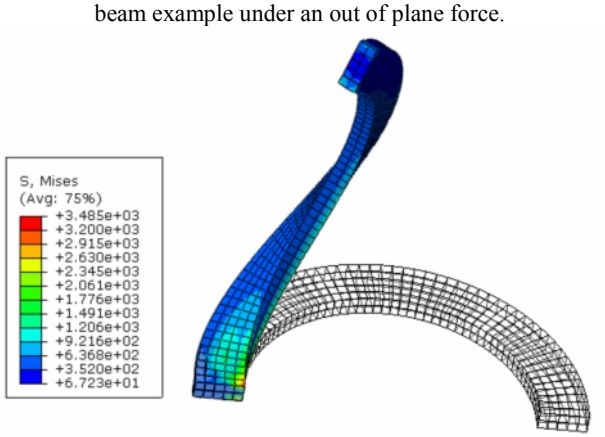

Figure 6. deformed shape under maximum force

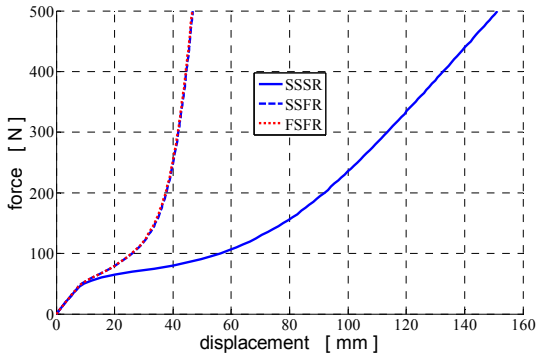

Figure 7. force-displacement diagram comparison for different formulations

Conclusions

In this study, we investigated a finite-strain constitutive model. The model development is based on the multiplicative decomposition of the deformation gradient into elastic and transformation parts. Time-discrete evolution equation and solution algorithm are discussed and implemented in a user-defined subroutine

UMAT in nonlinear finite element software ABAQUS. We simulated different boundary value problems and concluded that using a small-strain formulation without considering rotational effects can yield wrong results. We finally proposed to use a corotational formulation, as we showed that the obtained results are as accurate as the results for a full finite-strain formulations.

References

[1] Otsuka, K., and Wayman, C. M., 1998. Shape Memory Materials. Cambridge University Press, Cambridge.

[2] Duerig, T. W., Melton, K. N., Stoekel, D., and Wayman, C. M., 1990. Engineering Aspects of Shape Memory Alloys. Butterworth-Heinemann, London.

[3] Duerig, T., Pelton, A., and Stöckel, D., 1999. An overview of nitinol medical applications. Materials Science and Engineering A 273-275**,** 149-160.

[4] Funakubo, H., 1987. Shape Memory Alloys. Gordon and Breach Science Publishers, New York.

[5] Leclercq, S., Lexcellent, C., 1996. A general macroscopic description of the thermomechanical behavior of shape memory alloys. Journal of the Mechanics and Physics of Solids 44 (6), 953-957.

[6] Auricchio, F., Petrini, L., 2004a. A three-dimensional model describing stress-temperature induced solid phase transformations: solution algorithm and boundary value problems. International Journal for Numerical Methods in Engineering 61 (6), 807-836.

[7] Auricchio, F., Petrini, L., 2004b. A three-dimensional model describing stress-temperature induced solid phase transformations: thermomechanical coupling and hybrid composite applications. International Journal for Numerical Methods in Engineering 61 (5), 716-737.

[8] Arghavani, J., Auricchio, F., Naghdabadi, R., Reali, A., and Sohrabpour, S.,. A 3-D phenomenological constitutive model for shape memory alloys under multiaxial loadings, *International Journal of Plasticity* (in press).

[9] Bouvet, C., Calloch, S., Lexcellent, C., 2004. A phenomenological model for pseudoelasticity of shape memory alloys under multiaxial proportional and nonproportional loadings. European Journal of Mechanics - A/Solids 23 (1), 37-61.

[10] Helm, D., Haupt, P., 2003. Shape memory behaviour: modelling within continuum thermomechanics. International Journal of Solids and Structures 40 (4), 827-849.

[11] Souza, A.C., Mamiya, E.N., Zouain, N., 1998. Three-dimensional model for solids undergoing stress-induced phase transformations. European Journal of Mechanics - A/Solids 17 (5), 789-806.

[12] Reese, S., Christ, D., 2008. Finite deformation pseudo-elasticity of shape memory alloys - Constitutive modelling and finite element implementation. International Journal of Plasticity 24 (3), 455-482.

[13] Helm, D., 2001. Formgedachtnislegierungen – Experimentelle Untersuchung, phanomenologische Modellierung und numerische Simulation der thermomechanischen Materialeigenschaften. Ph.D. thesis, Universitat Gesamthochschule Kassel.

[14] Auricchio, F., Taylor, R.L., 1997. Shape-memory alloys: modelling and numerical simulations of the finite-strain superelastic behavior. Computer Methods in Applied Mechanics and Engineering 143 (1-2), 175-194.

[15] Evangelista, V., Marfia, S. and Sacco, E., 2009, A 3D SMA constitutive model in the framework of finite strain. International Journal for Numerical Methods in Engineering, in press.

[16] Muller, C., Bruhns, O.T., 2006. A thermodynamic finite-strain model for pseudoelastic shape memory alloys. International Journal of Plasticity 22, 1658–1682.

[17] Arghavani, J., in preparation. Thermomechanical behavior of shape memory alloys under nonproportional loading: Constitutive modelling and numerical inplementation in small and finite strains, *Ph.D. Thesis*, Sharif University of Technology, Iran.

[18] Arghavani, J., Auricchio, F., Naghdabadi, R., Reali, A. A robust and efficient integration algorithm for a 3D finite-strain SMA constitutive model, *submitted to International Jornal of Numerical Methods in Engineering*.